EXHIBIT M

Tapon et al., *Cell* 110: 467-478 (2002)

salvador Promotes Both Cell Cycle Exit and Apoptosis in *Drosophila* and Is Mutated in Human Cancer Cell Lines

Nicolas Tapon,[1,3] Kieran F. Harvey,[1] Daphne W. Bell,[1] Doke C.R. Wahrer,[1] Taryn A. Schiripo,[1] Daniel A. Haber,[1] and Iswar K. Hariharan[1,2]

[1]Massachusetts General Hospital Cancer Center
Building 149
13th Street
Charlestown, Massachusetts 02129
[2]Correspondence:
hariharan@helix.mgh.harvard.edu

[3]Present address: Institute of Signaling, Developmental Biology and Cancer, CNRS UMR 6543, Centre de Biochimie, Université de Nice, Parc Valrose, 06108 Nice, France.

Summary

The number of cells in an organism is determined by regulating both cell proliferation and cell death. Relatively few mechanisms have been identified that can modulate both of these processes. In a screen for *Drosophila* mutations that result in tissue overgrowth, we identified *salvador (sav)*, a gene that promotes both cell cycle exit and cell death. Elevated Cyclin E and DIAP1 levels are found in mutant cells, resulting in delayed cell cycle exit and impaired apoptosis. Salvador contains two WW domains and binds to the Warts (or LATS) protein kinase. The human ortholog of *salvador* (hWW45) is mutated in three cancer cell lines. Thus, *salvador* restricts cell numbers in vivo by functioning as a dual regulator of cell proliferation and apoptosis.

Introduction

The number of cells in an organism is determined by the number of cells generated as a result of cell proliferation as well the number of cells that are eliminated by cell death. Both cell proliferation and cell death are strictly regulated by developmental mechanisms to ensure that an organ of a characteristic shape and size is generated. The very mechanisms that regulate normal growth and cell proliferation are often those that are perturbed in human cancers. Mutational events found in cancers can either promote growth and cell proliferation or impede cell death.

The *Drosophila* compound eye is particularly suited to the application of genetic approaches to the study of cell proliferation and cell death in the context of organ development (Wolff and Ready, 1993). The adult eye develops from a primordium consisting of approximately 30 cells in the embryo. Cell growth and proliferation occur during all stages of larval development. Most of the cells generated adopt specialized fates (e.g., photoreceptor, pigment cell) during the late larval and pupal stages, leaving approximately 2000 unspecified cells. These excess cells are subsequently eliminated by a wave of apoptosis. Thus, the final number of cells in the adult eye can be altered by changes in either cell proliferation or cell death.

While the developmental signals that trigger cell cycle exit or apoptosis in *Drosophila* are still poorly characterized, considerable progress has been made in identifying the endpoints of these pathways. In many different tissues, cell cycle exit appears to be contingent on the downregulation of Cyclin E levels (Knoblich et al., 1994). This coincides with increased expression of the cdk inhibitor Dacapo during the final cell cycle (de Nooij et al., 1996; Lane et al., 1996). Dacapo inactivates residual Cyclin E/cdk2 complexes and facilitates a precisely timed exit from the cell cycle. The decrease in Cyclin E levels is primarily achieved by a reduction in its transcription, but other mechanisms including degradation of Cyclin E protein appear to be important (Jones et al., 2000; Moberg et al., 2001). Developmentally regulated cell death in the pupal retina is mediated by caspase activation. The Reaper, Hid, and Grim proteins bind to the *Drosophila* inhibitor of apoptosis 1 (DIAP1) protein and prevent DIAP1 from inhibiting caspases (Goyal et al., 2000; Lisi et al., 2000; Wang et al., 1999).

So far, relatively few mechanisms have been shown to be capable of regulating both cell proliferation and cell death in a coordinated manner. Using a phenotype-based screen in the

Cell Immediate Early Publication

Published Online July 12, 2002
DOI: 10.1016/S0092867402008243

Drosophila eye, we have identified *salvador* (*sav*), a gene that regulates both cell cycle exit and apoptosis. Here we present a phenotypic and molecular characterization of *sav* and show that its human ortholog is mutated in at least three cancer cell lines.

Results

To identify genes that restrict cell growth or cell numbers in vivo, we conducted a screen in the *Drosophila* eye for mutations that increase the relative representation of mutant tissue compared to wild-type tissue (Tapon et al., 2001). Using FLP/FRT-induced mitotic recombination, clones of mutant tissue (marked white) were compared in size to sister clones of wild-type tissue (marked red). We retained those flies whose eyes contained an excess of mutant over wild-type tissue. So far, we have identified mutations in at least 23 distinct loci that elicit this phenotype. These included negative regulators of cell proliferation such as *archipelago* (*ago*) as well as homologs of human tumor-suppressor genes including PTEN, TSC1, and TSC2 (Moberg et al., 2001; Tapon et al., 2001).

We identified three alleles of *sav*. A fourth allele, sav^4, was isolated by Jessica Treisman and was kindly provided to us. sav^1 and sav^2 generate eyes that have an increased representation of mutant tissue (white) over wild-type tissue (red) when compared to the parent chromosome (Figures 1A and 1B). sav^3 elicits a more severe phenotype; in addition to a further increase in the representation of mutant tissue, the mutant tissue protrudes from the eye in folds (Figures 1C–1E). sav^4 exhibits an intermediate phenotype. Clones of sav^3 mutant tissue generated in other parts of the fly including the notum and haltere also display outgrowths (Figures 1F and 1G). All four alleles are lethal when homozygous, in *trans* to each other or in *trans* to the deletion *Df(3R)hh* that spans the *sav* locus (see below).

In sav^1 clones in the adult retina, almost all the ommatidia contain the normal complement of eight photoreceptor cells. However, there is increased spacing between adjacent ommatidia (Figure 1H). In contrast to wild-type retinas from late pupae that contain a single layer of interommatidial cells (Figure 1I), mutant clones contain many additional interommatidial cells (Figure 1J). Generation of sav^1 mutant clones in a $white^+$ background indicated that most of these additional interommatidial cells contain pigment (data not shown). Thus, these cells can undergo terminal differentiation. The more disorganized retinas of the sav^3 allele display all of these phenotypic abnormalities. In addition, almost half of the ommatidia in sav^3 clones lack one or more photoreceptor cells.

sav Promotes Cell Cycle Exit

In wild-type imaginal discs, S phases, as visualized by BrdU incorporation, are observed anterior to the morphogenetic furrow (MF) and as a single stripe of incorporation posterior to the furrow referred to as the second mitotic wave (SMW) (Figure 2A). In *sav* clones, many BrdU-incorporating nuclei are observed posterior to the SMW (Figure 2B). Clones spanning the MF have some BrdU-incorporating nuclei in the anterior half of the MF (Figure 2C), a region that is normally composed of cells arrested in G1. Using the anti-phosphohistone H3 antibody, additional cells in mitosis are also visualized in *sav* mutant clones posterior to the MF, suggesting that at least some of these cells are completing additional cell cycles (Figures 2D and 2E). BrdU incorporation persists in mutant clones during the first 12 hr after puparium formation (APF) (Figure 2F) but has ceased by 24 hr APF (data not shown). Thus, *sav* mutant cells continue to proliferate for 12–24 hr after wild-type cells stop dividing but are eventually able to exit from the cell cycle and undergo terminal differentiation.

In cycling cells in the anterior portion of the eye imaginal disc, the distribution of mutant cells in the cell cycle, as assessed by flow cytometry, is extremely similar to that of wild-type cells (Figure 3A). The mutant cells are very slightly smaller than their wild-type counterparts. Posterior to the MF (Figure 3B), mutant populations have an increased proportion of cells in S and G2, indicating that mutant cells continue to cycle in this portion of the disc. Mutant cells are of normal size. The population doubling times of clones of mutant cells and wild-type cells generated in the wing imaginal disc during the proliferative phase of development (Figure 3C) did not differ

Cell Immediate Early Publication

Published Online July 12, 2002
DOI: 10.1016/S0092867402008243

significantly. Thus, when they are proliferating, mutant cells behave like wild-type cells. However, exit from the cell cycle is delayed in *sav* cells.

Elevated levels of Cyclin E protein are found in the basal nuclei of *sav* clones posterior to the MF (Figures 3D–3G). These are the nuclei of the undifferentiated cells that continue to proliferate in *sav* clones. We examined such discs for levels of *cyclin E* RNA. When *sav* clones are generated using *eyFLP* (Newsome et al., 2000), a large proportion of cells in third instar discs are mutant, and these discs contain large patches of mutant tissue. In wild-type discs, *cyclin E* RNA is expressed in a narrow stripe immediately posterior to the morphogenetic furrow (Figure 3H). In discs containing *sav* clones, the stripe of expression is broader and more intense, indicating that *cyclin E* RNA levels are elevated in these discs (Figure 3I). Thus, the increased level of Cyclin E protein is likely to result, at least in part, from an increase in *cyclin E* RNA levels.

sav Is Required for Apoptosis in the Eye Imaginal Disc

In wild-type eyes, excessive interommatidial cells are eliminated by a wave of apoptosis that is evident in 38 hr pupal retinas (Wolff and Ready, 1993). Even in *sav* mutant clones, cell proliferation, as assessed by BrdU incorporation, has ceased within 24 hr APF. When mosaic retinas were examined 38 hr APF, cell death is mostly confined to the wild-type portions of the retina (Figures 2G–2I). Thus, the apoptotic cell deaths that are part of normal retinal development appear to require *sav* function.

Apoptosis in the pupal retina requires *hid* function, since *hid* mutants display additional interommatidial cells (Kurada and White, 1998). Hid is thought to induce caspase activation by binding to the DIAP1 protein and preventing it from inhibiting caspase function (Goyal et al., 2000; Lisi et al., 2000; Wang et al., 1999). Overexpression of *hid* using the eye-specific GMR promoter generates a small eye (Figure 4A; Hay et al., 1995). The induction of cell death by *hid* is severely impaired in *sav* mutant clones (Figures 4M–4O). As a consequence, eyes derived from *GMR-hid*-expressing discs that contain *sav* mutant clones are larger than those derived from wild-type discs that express *GMR-hid* (Figures 4A and 4B). Since *sav* function is required for *hid*-induced cell death, *sav* is likely to function either downstream of *hid* or in a parallel pathway.

Several very recent studies have shown that another mechanism by which Hid and Rpr activate caspases is by inducing the autoubiquitination of DIAP1 and targeting it for degradation by the proteasome (Hays et al., 2002; Holley et al., 2002; Ryoo et al., 2002; Wilson et al., 2002; Wing et al., 2002; Yoo et al., 2002). We found that DIAP1 levels are markedly elevated in *sav* clones in the larval eye disc (Figures 4C and 4D) and remain elevated in the interommatidial cells in mutant clones in the pupal eye disc (Figures 4E and 4F) where we have observed a reduction of apoptosis (Figures 2H and 2I). Thus, increased levels of DIAP1 in *sav* cells may be able to overcome the effect of many proapoptotic signals.

To examine DIAP1 RNA levels, we used in situ hybridization to examine 20 wild-type discs and 20 mutant discs. The presence of *sav* (GFP^-) clones in the mutant discs was confirmed by examining the discs by fluorescence microscopy prior to hybridization. There is a modest level of DIAP1 RNA expression posterior to the furrow in both populations of discs (Figures 4K and 4L) and no evidence of increased DIAP1 RNA in the discs containing *sav* clones. Thus, at least at this level of detection, the increased DIAP1 expression in *sav* cells does not appear to result from increased transcription.

In wild-type eye discs, DIAP1 protein is expressed at higher levels posterior to the morphogenetic furrow (Figure 4G). DIAP1 protein levels are downregulated by *GMR-rpr* (Figure 4H) or, to a lesser extent, by *GMR-hid* expression (data not shown). In *sav* mutant clones expressing *GMR-rpr*, DIAP1 protein levels remain elevated (Figures 4I and 4J). Similar results are observed with *GMR-hid* (data not shown). Thus, neither *GMR-rpr* nor *GMR-hid* appears capable of downregulating the elevated levels of DIAP1 sufficiently in *sav* clones to activate caspases.

Expression of *hid* or *reaper* (*rpr*) in the eye imaginal disc results in activation of the effector

Cell Immediate Early Publication

Published Online July 12, 2002
DOI: 10.1016/S0092867402008243

caspase Drice. An antibody that recognizes the cleaved (activated) form of Drice (Yoo et al., 2002) was used to stain eye discs expressing *GMR-hid* or *GMR-rpr*. In wild-type cells, Drice is activated by *GMR-hid* (Figure 4P) or *GMR-rpr* (Figure 4S). However, in clones of *sav* tissue, Drice activation by either *GMR-hid* (Figures 4Q and 4R) or *GMR-rpr* (Figures 4T and 4U) is almost completely blocked. To counteract the possibility of convolutions in the disc, the stainings shown are projections of confocal Z series (12 individual frames) spanning the entire thickness of the eye disc, excluding the peripodial membranes. At least 30 discs per genotype from three independent experiments were carefully examined to confirm the results. These experiments indicate that *sav* blocks activation of Drice by both *rpr* and *hid*.

A mutant form of Hid (Hid-Ala5) is resistant to inactivation by MAP kinase phosphorylation (Bergmann et al., 1998). *GMR-hid-Ala5* is a more potent inducer of cell death, as assessed by the extent of Drice activation (Figure 4V) in the eye disc, than is *GMR-hid* (Figure 4P). Cell death induced by *GMR-hid-Ala5* is only partially blocked in *sav* clones (Figures 4W and 4X), indicating that the increased potency of Hid-Ala-5 may be able to overcome increased DIAP1 levels.

sav Encodes a Protein with WW Domains and Has a Human Ortholog

The *sav* mutations were localized to the interval 93F11-13 to 94D10-13. High-resolution meiotic mapping localized *sav* to a 20 kb region that contained five ORFs (Figure 5A and Experimental Procedures). We sequenced all five ORFs completely and found that all four *sav* chromosomes had truncating mutations in CG13831. The other four ORFs did not have any amino acid changes. We examined five independent cDNA clones of CG13831 by restriction mapping, and two independent clones were sequenced completely. The longest clone is 2.2 kb long, which is in agreement with the approximate size of the RNA determined by Northern blotting (Figure 5B). The predicted ORF, encoding a protein of 608 amino acids (Figures 5C and 5D), includes the entire coding region since there is a stop codon upstream and in-frame with the ATG codon. The predicted Sav protein has two WW domains, and its C-terminal portion includes a domain that is likely to adopt the conformation of a coiled-coil. Sav is most similar to the human protein hWW45 (Valverde, 2000) and to the protein encoded by the *C. elegans* ORF T10H10.3 (Figure 5D). WW domains are known to mediate protein-protein interactions with various proline-containing motifs (Kato et al., 2001). The more C-terminal WW domain lacks the second conserved tryptophan residue that is required for substrate binding and is unlikely to be a functional WW domain. The N-terminal WW domain contains all of the appropriate conserved residues. This putative WW domain is predicted to belong to the Group I family of WW domains that is predicted to interact with the PPXY ("PY") motif.

The mutations in sav^1, sav^2, and sav^4 result in stop codons in positions 289, 231, and 160, respectively, that would truncate the protein N-terminal to the WW domains (Figure 5). As expected, the more N-terminally located sav^4 mutation has a more severe phenotype than sav^1 or sav^2. Surprisingly, the sav^3 mutation, which elicits the most severe phenotype, maps 3′ to those found in sav^1 and sav^2. The sav^3 mutation causes a frameshift and generates a protein consisting of 406 *sav*-encoded amino acids and a C-terminal portion of 84 amino acids derived from the use of an alternate open reading frame that has no sequence similarity to any protein in the database. It is possible that sav^1, sav^2, and sav^4 proteins may have some residual activity despite the absence of the WW domains and that sav^3 is a null allele. The sav^3 allele may have a more severe phenotype because the novel C-terminal sequences may further impair its stability or function. Alternatively, the novel C terminus of the sav^3 protein may confer some neomorphic properties. Any such properties, if present, are not apparent in the presence of the wild-type protein, since sav^3/+ flies display no overt phenotypic abnormalities. We also found that in different transheterozygous combinations, sav^3 is similar in strength to a deletion. In four independent experiments, sav^1/sav^3 animals and $sav^1/Df(3R)EB6$ animals have hatching rates of 85.5% (SD 2.5%) and 83.3% (SD 3.2%),

Cell Immediate Early Publication

Published Online July 12, 2002
DOI: 10.1016/S0092867402008243

respectively (n = 40), and 90%–95% of the animals of each genotype subsequently failed to grow and died as first instar larvae. Thus, at least by this criterion, sav^3 behaves like a null mutation. Importantly, the abnormalities in cell proliferation and apoptosis were analyzed using at least two different *sav* alleles and only quantitative differences were observed between sav^3 and the weaker alleles.

In the eye disc, *sav* is expressed in a stripe in the MF, and expression decreases in the region of the SMW (Figures 2J and 2K). Expression increases once again posterior to the SMW. Thus, to a first approximation, *sav* expression coincides with regions of temporary or permanent cell cycle arrest and supports the notion that *sav* functions in promoting exit from the cell cycle.

sav Functions together with *warts*

A candidate for a Sav-interacting protein is encoded by the *warts* (*wts*; also known as *LATS*) gene (Bryant et al., 1993; Justice et al., 1995; Xu et al., 1995) that encodes a serine-threonine kinase. Clones of *wts* tissue generate outgrowths that resemble tumors. We identified nine alleles of *wts* in our screen, and the phenotype of sav^3 is similar to that elicited by hypomorphic mutations in *wts*. Null alleles of *wts* display a more severe phenotype. Like *sav*, *wts* clones in the pupal retina have additional interommatidial cells (Figure 6A). Larval imaginal discs containing large *wts* clones are enlarged and convoluted (Justice et al., 1995; Xu et al., 1995). Larval eye discs that contain *eyFLP*-induced *wts* clones are composed mostly of mutant tissue with small regions of wild-type tissue. Many additional BrdU-incorporating nuclei are observed in mutant clones posterior to the SMW (Figure 6B). As observed with *sav*, the stripe of *cyclin E* RNA expression is also broadened in these discs (Figure 6C). Moreover, the normal cell death that occurs in the pupal retina is almost completely abolished in *wts* mutant clones (Figure 6D). Thus, as for *sav*, *wts* mutations generate additional interommatidial cells resulting from both increased cell proliferation posterior to the SMW as well as reduced apoptosis in the pupal retina. In addition, Drice activation induced by *GMR-hid* is markedly diminished in *wts* clones (Figures 6E and 6F).

Overexpression of *sav* alone using the GMR promoter (Hay et al., 1995) has no effect (Figure 6G), and overexpression of *wts* generates subtle irregularities in ommatidial architecture (Figure 6H). However, combined overexpression of *sav* and *wts* results in a smaller eye where the ommatidial pattern is highly irregular (Figure 6I). This effect appears to reflect a synergistic increase in cell death in the eye discs of flies that express both transgenes (Figures 6J–6M) as well as a minor effect on reducing cell proliferation associated with the SMW (data not shown).

Thus, Sav and Wts may function in the same pathway and may bind to each other. Indeed, the Sav protein has a Group I WW domain that is predicted to interact with the PPXY (PY) motif (Kato et al., 2001), five of which are found in the Wts protein. To test whether *Drosophila* Sav and Wts proteins could physically interact, a GST pull-down assay was employed (Figure 6N). The region containing the two potential WW domains of Sav was fused to GST and incubated with cell lysates that expressed Myc-tagged Wts protein. Using this assay, Wts was found to interact specifically with the region of Sav that contained the WW domain. Furthermore, a 15 amino acid peptide, designed to mimic one of the PY motifs of Wts, was found to inhibit the interaction between the WW domain region of Sav and Wts. An identical peptide where the tyrosine residue that is required for interaction with type I WW domains had been replaced by an alanine did not prevent this interaction. Thus, at least under the conditions of this experiment, Sav and Wts interact in a WW domain- and PY motif-dependent fashion, suggesting that an analogous interaction could occur in vivo.

Discs containing clones of the *wts* null allele, wts^{latsX1} (Xu et al., 1995), are much larger than discs containing sav^3 clones. If all *sav* functions were *wts* dependent, the double mutant phenotype should not be more severe than the *wts* phenotype. When mutant clones were generated with *eyFLP*, average disc sizes were 39,669 pixels (SD 10,401) for sav^3, wts^{latsX1} double mutant discs and 31,360 pixels (SD 5260) for wts^{latsX1} discs (n = 20). Thus, the double mutant discs were significantly larger than the wts^{latsX1} discs ($p < 0.01$). Thus, while *sav* and *wts* appear to function together in certain ways, they

Cell Immediate Early Publication

Published Online July 12, 2002
DOI: 10.1016/S0092867402008243

are also likely to have functions that are independent of each other.

The Human Ortholog of *sav*, hWW45, Is Mutated in Cancer Cell Lines

Since mutations in *sav* lead to excessive cell proliferation and reduced cell death, we tested whether hWW45 might be a mutational target in cancer. hWW45 maps to the chromosomal region 14q13–14q23 (Valverde, 2000), a locus that is subject to allelic loss in a variety of cancers, including renal cancers, ovarian cancers, and malignant mesothelioma. We sequenced the entire coding region of hWW45 in a panel of 52 tumor-derived cell lines, representing a broad range of tissue types. One colon cancer cell line, HCT15, had a heterozygous C to A mutation at nucleotide 554, resulting in a substitution of aspartic acid for alanine at codon 185. This mutation was not present in 185 population-based controls (370 chromosomes), indicating that it is not a common polymorphism. HCT15 carries a mutation in the mismatch repair gene MSH6, which appears to enhance the frequency of point mutations in other genes. More significantly, two renal cancer cell lines, ACHN and 786-O, were found to have deletions involving hWW45. The normal allele was not present in either cell line, indicating that these cell lines are either homozygous or hemizygous for the deletion. The hWW45 transcript was undetectable by RT-PCR in both cell lines, and a Southern blot using a probe derived from the 3′ portion of the gene demonstrated that this part of the gene was absent in both cell lines (Figure 7A). In cell line 786-O, PCR analysis of genomic DNA indicated that there is a deletion of ?157 kb with the 5′ breakpoint between exons 2 and 3 of hWW45. The deletion in ACHN of ?138 kb encompassed the entire gene (Figure 7B). The common region of overlap between these two deletions is only 21 kb, containing exons 3–5 of hWW45. No other transcription units were identified within this 21 kb interval, using the GENSCAN exon prediction program. Thus, we have identified deletions that would inactivate the human ortholog of *sav* in at least two cancer cell lines.

Discussion

Role of *sav* in Promoting Cell Cycle Exit

In the eye disc, *sav* clones contain cells that continue to proliferate for 12–24 hr (Figure 2) after their normal counterparts stop dividing. Our studies of cycling cells show almost no differences between wild-type and mutant populations (Figure 3). However, given that mutant clones contain more ommatidia than wild-type twin spots, accelerated growth must have occurred in mutant tissue anterior to the furrow. Even a relatively minor growth advantage exhibited by mutant cells at every cell cycle can eventually result in increased clone size when amplified by the approximately nine rounds of cell division that occur in the eye primordium prior to the passage of the MF. A subtle change in cell cycle parameters may not easily be detected.

In *sav* clones, elevated Cyclin E protein levels are observed in the basal nuclei posterior to the MF in the eye imaginal disc (Figure 3). These cells normally stop dividing when they downregulate Cyclin E protein levels. In discs containing many *sav* clones, the stripe of *cyclin E* RNA expression is broader and more intense. Thus, the increased level of Cyclin E protein is, at least in part, a result of elevated *cyclin E* RNA levels. Thus, an inability to downregulate Cyclin E/cdk activity may be the result of increased levels of *cyclin E* RNA as occurs in *sav* clones, impaired protein degradation (Moberg et al., 2001), or reduced levels of the cdk inhibitor Dacapo (de Nooij et al., 1996; Lane et al., 1996). In each case, cell cycle exit is delayed.

Role of *sav* in Regulating Cell Death

Elevated DIAP1 levels are likely to underlie the absence of the developmentally regulated apoptosis in *sav* clones in the pupal retina (Figure 4) as well as the resistance to *hid*-induced and *rpr*-induced apoptosis in the larval imaginal disc. The elevated DIAP1 levels appear to result from alterations in posttranscriptional regulation of DIAP1 expression. Recent work has shown that both Rpr and Hid can

Cell Immediate Early Publication

Published Online July 12, 2002
DOI: 10.1016/S0092867402008243

downregulate DIAP1 levels either by promoting the autoubiquitination of DIAP1 or by causing a generalized inhibition of translation that especially impacts proteins with a short half-life such as DIAP1 (Hays et al., 2002; Holley et al., 2002; Ryoo et al., 2002; Wilson et al., 2002; Wing et al., 2002; Yoo et al., 2002). Either of these mechanisms is likely to be less efficient in cells that already have elevated levels of DIAP1.

Our findings indicate that Sav normally functions to downregulate the basal level of DIAP1 protein. In the absence of Sav, higher levels of DIAP1 accumulate. This increases the level of Hid or Rpr activity that is required to overcome DIAP1-mediated inhibition of caspase activation. Consistent with this model, the more potent form of Hid, Hid-Ala5, is able to partially overcome the increased levels of DIAP1 in *sav* clones and induce a low level of caspase activity.

Sav appears capable of regulating both cell cycle exit and apoptosis by virtue of its ability to modulate the levels of two key regulators—Cyclin E and DIAP1. Loss of *sav* appears to increase *cyclin E* levels transcriptionally and DIAP1 levels by a posttranscriptional mechansim. Since cell number is determined by both the extent of cell proliferation as well as apoptosis, *sav* could function as a key regulator of cell number by virtue of its ability to regulate both processes.

One of few pathways that can directly regulate both cell proliferation and cell death is the Ras/MAPK pathway. Ras can promote cell proliferation by promoting growth (Prober and Edgar, 2000), and MAP kinase can phosphorylate and inactivate Hid and also reduce Hid transcription (Bergmann et al., 1998; Kurada and White, 1998). Our results indicate that *sav* might function in a distinct pathway. First, no change in diphospho-ERK activity is observed in *sav* mutant clones. Second, cell death induced by the MAP kinase-resistant Hid-Ala5 protein (where five putative MAPK phosphorylation sites have been mutated to alanines) is also reduced by a loss of *sav* function. However, it is still possible that *sav* might function downstream of the MAPK family proteins.

Interaction between Sav and Wts

Clones of cells mutant for *wts* generate large tumor-like growths in *Drosophila* (Bryant et al., 1993; Justice et al., 1995; Xu et al., 1995). Its human ortholog LATS1 binds to the cdc2 protein kinase in a cell cycle-dependent manner and inhibits its activity (Tao et al., 1999). Thus, it has been suggested that excessive Cyclin A/cdc2 may cause excessive cell proliferation by promoting both the G1/S and G2/M transitions. The interaction between *wts* and *cdc2*, however, does not explain the excessive and inappropriate growth (mass accumulation) that appears to drive the cell proliferation in clones of *wts* mutant cells. The defect in cell death in *wts* cells is also not easily accounted for by the interaction of Wts with cdc2. Our data raise the possibility that *sav* and *wts* might interact (via a WW domain-PY motif-dependent interaction) and function to promote cell cycle exit and apoptosis during development. However, *wts* is likely to have *sav*-independent functions as well. While *sav* mutations appear to result in a subtle increase in growth rate, the very strong overrepresentation of *wts* mutant tissue in third instar larval discs indicates that *wts* mutations must cause a much greater increase in growth rate.

sav and *wts* Orthologs as Tumor Suppressors in Humans

Mice lacking the *warts* ortholog LATS1 display pituitary hyperplasia and develop slow-growing tumors (St John et al., 1999). This contrasts with the dramatic overgowth phenotype observed in *wts* mutants in *Drosophila*. These differences may be due to the presence of other *wts* homologs (e.g., LATS2) in mammals that can partially compensate for LATS1 inactivation (St John et al., 1999).

The presence of a single *sav* homolog, hWW45, in humans makes it less likely that its function is redundant with that of a related gene. We have already identified mutations in this gene in three cancer cell lines and shown that two of these cell lines have homozygous deletions that either disrupt or eliminate the gene (Figure 7). While cell lines can accumulate mutations in culture, our findings nevertheless represent a first step in implicating hWW45 in the pathogenesis of human cancer.

Cell Immediate Early Publication

Published Online July 12, 2002
DOI: 10.1016/S0092867402008243

Concluding Remarks

Although chromosomal aberrations have been consistently identified for a number of human tumors, in most cases the relevant lesion has not been molecularly characterized. Many mammalian tumor suppressor genes must exist that have not yet been identified. Our phenotype-based screen, which is capable of detecting even subtle increases in growth or cell proliferation, has identified a number of genes that restrict growth or cell number. For *ago* and *sav*, we have subsequently identified mutations in their human orthologs in cancer cell lines. Thus, the strategy of conducting phenotype-based screens in model organisms followed by a search for mutations in cancer cell lines may help us to identify new tumor suppressor genes.

Experimental Procedures

Fly Stocks

w; FRT82B males were mutagenized with ethylmethanesulfonate (EMS), then crossed either to *y w eyFLP; FRT82B P[mini-w, armLacZ]* or first to *w; TM3/TM6B* and then individually to *y w eyFLP; FRT82B P[mini-w, armLacZ]* (Tapon et al., 2001). Males with mostly white eyes were retained and maintained as balanced stocks. Alleles of *sav* identified were sav^{1}, sav^{2}, and sav^{3}. *GMR-hid* and *2XGMR-rpr* (on the second chromosome) were from Kristin White. *GMR-hid Ala5* (second chromosome) was from Andreas Bergmann. *FRT82B* $LATS^{X1}$ has been described (Xu et al., 1995). wts^{MGH1}, identified in our screen, is a homozygous lethal allele of moderate strength.

Mapping

sav mutations fail to complement the lethality of *Df(3R)hh*, which deletes 93F11-13 to 94D10-13. Using P element-mediated male recombination, the sav^{1} allele was placed in *cis* to P[lacW]C2-3-33 at 94D. We placed the P[lacW]C2-3-33, sav^{1} chromosome in *trans* to the P[EP]3251 (distal to *sav*) chromosome in females. We selected for meiotic recombination events between the two P elements. We then identified a SNP 57 kb proximal to P[EP]3251 (Figure 2A). Some crossovers proximal to the SNP were sav^{+}, indicating that *sav* was proximal to the SNP. Of the sav^{+} lines, 14 of 19 lines had the polymorphic variant from the P[EP]3251 chromosome, while 5 of 19 had the sav^{1} chromosome version. Since the SNP was 57 kb away from P[EP]3251, *sav* was likely to be located approximately 20 kb proximal to the SNP. We sequenced genomic DNA from the *sav* chromosomes for five predicted ORFs in this region (Figure 5A). We found that all these ORFs were wild-type except CG13831, which had a nonsense mutation in each *sav* chromosome.

Microscopy, Immunohistochemistry, Flow Cytometry

For adult eye pictures, sections, and eye SEMs, genotypes were as follows: *y w, eyFLP/+; FRT82B /FRT82B P[mini-w] P[armLacZ]* and *y w, eyFLP/+; FRT82B* $sav^{1/3}$ */FRT82B P[mini-w] P[armLacZ]*. For thorax SEMs, genotypes were *y w, hsFLP/+; FRT82B / FRT82B P[πMyc] P[w y]* and *y w, hsFLP/+; FRT82B* sav^{3} */ FRT82B P[πMyc] P[w y]*.

Imaginal disc BrdU incorporations used a 1.5 hr BrdU pulse to visualize ectopic S phases posterior to the MF. Antibodies used were anti-rabbit-Cy5 and anti-mouse Cy3 (Jackson Laboratories), a rabbit polyclonal anti-phosH3 antibody (Upstate Laboratories), anti-β-galactosidase rabbit polyclonal (Cappel), a mouse monoclonal anti-β-galactosidase (Promega), and a mouse monoclonal anti-DIAP1 antibody and a rabbit anti-activated Drice antibody (both from Bruce Hay) (Yoo et al., 2002). FACS analysis was performed as described previously (Neufeld et al., 1998; Tapon et al., 2001).

For immunofluorescence and TUNEL stainings, discs were dissected from the following genotypes: (1) *y w, eyFLP/+; FRT82B* $sav^{1/2/3}$ */FRT82B P[mini-w] P[armLacZ]*, (2) *y w eyFLP/+; FRT82B* wts^{MGH1}*/FRT82B P[mini-w] P[armLacZ]*, and (3) *y w eyFLP/+; FRT82B LATSX1/ FRT82B P[mini-w] P[armLacZ]*. For TUNEL, DIAP1, or Drice stainings and adult eye pictures in a *GMR-hid* transgenic background, genotypes were *y w, eyFLP/+;*

Cell Immediate Early Publication

Published Online July 12, 2002
DOI: 10.1016/S0092867402008243

GMR hid/+; FRT82B /FRT82B P[mini-w] P[armLacZ] and *y w, eyFLP/+; GMR hid/+; FRT82B sav^3 /FRT82B P[mini-w] P[armLacZ]*. For DIAP1 or Drice in a *GMR-rpr* or *GMR-hid-Ala5* transgenic background, genotypes were *y w, eyFLP/+; GMR hid/+; FRT82B /FRT82B P[mini-w] P[armLacZ]* and *y w, eyFLP/+; GMR hidAla5* (or *2XGMRrpr)/+; FRT82B sav^3 /FRT82B P[mini-w] P[UbiGFP]*. TUNEL stainings were performed as previously described (Kurada and White, 1998). TUNEL positive nuclei were detected with a Rhodamine-conjugated anti-DIG antibody (Boerhinger). For FACS analysis, the genotype was *y w, eyFLP/+; FRT82B sav^3 /FRT82B P[mini-w] P[UbiGFP]*.

Loss-of-function wing clone counts were performed as previously described (Tapon et al., 2001). Clones were induced at 48 hr after egg deposition (AED). Discs were dissected for analysis at 120 hr AED. The genotype was *y w, hsFLP/+; FRT82B sav^3 /FRT82B P[mini-w] P[UbiGFP]*.

Molecular Biology

The coding region of a *sav* cDNA clone was PCR amplified using oligonucleotide primers with *EcoRI* and *BglII* sites and cloned into pGMR. A 4.1 kb *EcoRI/DraI* fragment of the *wts* cDNA (from Peter Bryant) was cloned into pGMR. *GMR-sav* and *GMR-wts* were third chromosome integrations.

Characterization of Human hWW45

The entire coding region of hWW45 was amplified by RT-PCR in two overlapping fragments. Uncloned PCR products were sequenced directly. The cancer cell lines analyzed and the DNA used for control populations are described in Moberg et al. (2001).

Primers derived from intronic sequences were used to amplify individual exons of hWW45 from genomic DNA of the ACHN and 780-O cell lines to assess the extent of genomic deletions in these two cases. For the regions flanking hWW45, primers based on nonrepetitive sequences from BACs containing hWW45 were used.

Protein Binding Studies

The *Drosophila warts* gene was Myc tagged and cloned into the pCDNA3 mammalian expression vector. The Salvador WW domain-GST construct was generated by cloning sequences encoding residues 419–495 into the *Bam*HI/*Eco*RI sites of pGEX-2TK. 293T cells were transfected using Fugene and harvested 36 hr later in lysis buffer (50 mM Tris-HCl [pH 7.5], 150 mM NaCl, 10 mM EDTA, 10% glycerol, 1% Triton X-100, 20 mg/ml leupeptin, 10 mg/ml aprotitin, 1 mM PMSF, 0.5 mM DTT, 0.5 mM NaF). Cell lysates were incubated with 500 ng to 1 mg of GST-fusion protein coupled to glutathione-sepharose, in the presence or absence of peptides (1 mM) for 2 hr at 4°C. Peptides were PY-GRQMLPPPPYQSNNN and PA-GRQMLPPPPAQSNNN. Beads were then washed, treated with protein sample buffer, and subjected to SDS-PAGE. Wts protein was detected by immunoblotting with anti-Myc tag 9E10 mAb.

Acknowledgments

We thank W. Fowle for generating the SEMs; A. Bergmann, P. Bryant, B. Hay, Y. Hiromi, J. Mohler, J. Treisman, K. White, T. Xu, and V. Yajnik for fly stocks, antibodies, and reagents; J. Jetz-Arruda for help with FACS analysis; G. Waneck for help with confocal microscopy; S. Schelble, K. Graber, K. Moberg, and B. Pellock for help with experiments; L. Aravind for help with sequence comparisons; and N. Dyson and K. White for comments on the manuscript. N.T. thanks P. Leopold for support. N.T. was funded by an HFSP long-term fellowship, and I.K.H. was funded in part by the NIH (GM61672 and EY11632) and is a Faculty Scholar of the Richard Saltonstall Foundation. D.W.B, D.C.R.W., and D.A.H. are funded in part by the NIH (CA87691), the SPORE in breast cancer at MGH, the Avon foundation, and the AACR-NFCR Professorship (D.A.H.).

Received: February 15, 2002

Revised: June 27, 2002

Published online: July 12, 2002

Published Online July 12, 2002
DOI: 10.1016/S0092867402008243

References

Bergmann, A., Agapite, J., McCall, K., and Steller, H. (1998). The *Drosophila* gene hid is a direct molecular target of Ras-dependent survival signaling. Cell *95*, 331–341.

Bryant, P.J., Watson, K.L., Justice, R.W., and Woods, D.F. (1993). Tumor suppressor genes encoding proteins required for cell interactions and signal transduction in *Drosophila*. Dev. *Suppl*, 239–249.

de Nooij, J.C., Letendre, M.A., and Hariharan, I.K. (1996). A cyclin-dependent kinase inhibitor, Dacapo, is necessary for timely exit from the cell cycle during *Drosophila* embryogenesis. Cell *87*, 1237–1247.

Goyal, L., McCall, K., Agapite, J., Hartwieg, E., and Steller, H. (2000). Induction of apoptosis by *Drosophila* reaper, hid and grim through inhibition of IAP function. EMBO J. *19*, 589–597.

Hay, B.A., Wassarman, D.A., and Rubin, G.M. (1995). *Drosophila* homologs of baculovirus inhibitor of apoptosis proteins function to block cell death. Cell *83*, 1253–1262.

Hays, R., Wickline, L., and Cagan, R. (2002). Morgue mediates apoptosis in the *Drosophila melanogaster* retina by promoting degradation of DIAP1. Nat. Cell Biol. *4*, 425–431.

Holley, C.L., Olson, M.R., Colon-Ramos, D.A., and Kornbluth, S. (2002). Reaper eliminates IAP proteins through stimulated IAP degradation and generalized translational inhibition. Nat. Cell Biol. *4*, 439–444.

Jones, L., Richardson, H., and Saint, R. (2000). Tissue-specific regulation of cyclin E transcription during *Drosophila melanogaster* embryogenesis. Development *127*, 4619–4630.

Justice, R.W., Zilian, O., Woods, D.F., Noll, M., and Bryant, P.J. (1995). The *Drosophila* tumor suppressor gene warts encodes a homolog of human myotonic dystrophy kinase and is required for the control of cell shape and proliferation. Genes Dev. *9*, 534–546.

Kato, Y., Ito, M., Kawai, K., Nagata, K., and Tanokura, M. (2001). Determinants of ligand specificity in groups I and IV WW domains as studied by surface plasmon resonance and model building. J. Biol. Chem. *277*, 10173–10177.

Knoblich, J.A., Sauer, K., Jones, L., Richardson, H., Saint, R., and Lehner, C.F. (1994). Cyclin E controls S phase progression and its down-regulation during *Drosophila* embryogenesis is required for the arrest of cell proliferation. Cell *77*, 107–120.

Kurada, P., and White, K. (1998). Ras promotes cell survival in *Drosophila* by downregulating hid expression. Cell *95*, 319–329.

Lane, M.E., Sauer, K., Wallace, K., Jan, Y.N., Lehner, C.F., and Vaessin, H. (1996). Dacapo, a cyclin-dependent kinase inhibitor, stops cell proliferation during *Drosophila* development. Cell *87*, 1225–1235.

Lisi, S., Mazzon, I., and White, K. (2000). Diverse domains of THREAD/DIAP1 are required to inhibit apoptosis induced by REAPER and HID in *Drosophila*. Genetics *154*, 669–678.

Moberg, K.H., Bell, D.W., Wahrer, D.C., Haber, D.A., and Hariharan, I.K. (2001). Archipelago regulates Cyclin E levels in *Drosophila* and is mutated in human cancer cell lines. Nature *413*, 311–316.

Neufeld, T.P., de la Cruz, A.F., Johnston, L.A., and Edgar, B.A. (1998). Coordination of growth and cell division in the *Drosophila* wing. Cell *93*, 1183–1193.

Newsome, T.P., Asling, B., and Dickson, B.J. (2000). Analysis of *Drosophila* photoreceptor axon guidance in eye-specific mosaics. Development *127*, 851–860.

Prober, D.A., and Edgar, B.A. (2000). Ras1 promotes cellular growth in the *Drosophila* wing. Cell *100*, 435–446.

Ryoo, H.D., Bergmann, A., Gonen, H., Ciechanover, A., and Steller, H. (2002). Regulation of *Drosophila* IAP1 degradation and apoptosis by reaper and ubcD1. Nat. Cell Biol. *4*, 432–438.

Cell Immediate Early Publication

Published Online July 12, 2002
DOI: 10.1016/S0092867402008243

St John, M.A., Tao, W., Fei, X., Fukumoto, R., Carcangiu, M.L., Brownstein, D.G., Parlow, A.F., McGrath, J., and Xu, T. (1999). Mice deficient of Lats1 develop soft-tissue sarcomas, ovarian tumours and pituitary dysfunction. Nat. Genet. *21*, 182–186.

Tao, W., Zhang, S., Turenchalk, G.S., Stewart, R.A., St John, M.A., Chen, W., and Xu, T. (1999). Human homologue of the *Drosophila melanogaster* lats tumour suppressor modulates CDC2 activity. Nat. Genet. *21*, 177–181.

Tapon, N., Ito, N., Dickson, B.J., Treisman, J.E., and Hariharan, I.K. (2001). The *Drosophila* tuberous sclerosis complex gene homologs restrict cell growth and cell proliferation. Cell *105*, 345–355.

Valverde, P. (2000). Cloning, expression, and mapping of hWW45, a novel human WW domain-containing gene. Biochem. Biophys. Res. Commun. *276*, 990–998.

Wang, S.L., Hawkins, C.J., Yoo, S.J., Muller, H.A., and Hay, B.A. (1999). The *Drosophila* caspase inhibitor DIAP1 is essential for cell survival and is negatively regulated by HID. Cell *98*, 453–463.

Wilson, R., Goyal, L., Ditzel, M., Zachariou, A., Baker, D.A., Agapite, J., Steller, H., and Meier, P. (2002). The DIAP1 RING finger mediates ubiquitination of Dronc and is indispensable for regulating apoptosis. Nat. Cell Biol. *4*, 445–450.

Wing, J.P., Schreader, B.A., Yokokura, T., Wang, Y., Andrews, P.S., Huseinovic, N., Dong, C.K., Ogdahl, J.L., Schwartz, L.M., White, K., and Nambu, J.R. (2002). *Drosophila* Morgue is an F box/ubiquitin conjugase domain protein important for grim-reaper mediated apoptosis. Nat. Cell Biol. *4*, 451–456.

Wolff, T., and Ready, D.F. (1993). Pattern formation in the *Drosophila* retina. In The Development of *Drosophila melanogaster*, M. Bate, and A. Martinez Arias, eds. (Plainview, New York: Cold Spring Harbor Laboratory Press), pp. 1277–1325.

Xu, T., Wang, W., Zhang, S., Stewart, R.A., and Yu, W. (1995). Identifying tumor suppressors in genetic mosaics: the *Drosophila* lats gene encodes a putative protein kinase. Development *121*, 1053–1063.

Yoo, S.J., Huh, J.R., Muro, I., Yu, H., Wang, L., Wang, S.L., Feldman, R.M., Clem, R.J., Muller, H.A., and Hay, B.A. (2002). Hid, Rpr and Grim negatively regulate DIAP1 levels through distinct mechanisms. Nat. Cell Biol. *4*, 416–424.

Accession Numbers

The GenBank accession number for the *sav* cDNA sequence was not available at the time of this online publication and will appear in the print version of this article.

Cell Immediate Early Publication

Published Online July 12, 2002
DOI: 10.1016/S0092867402008243

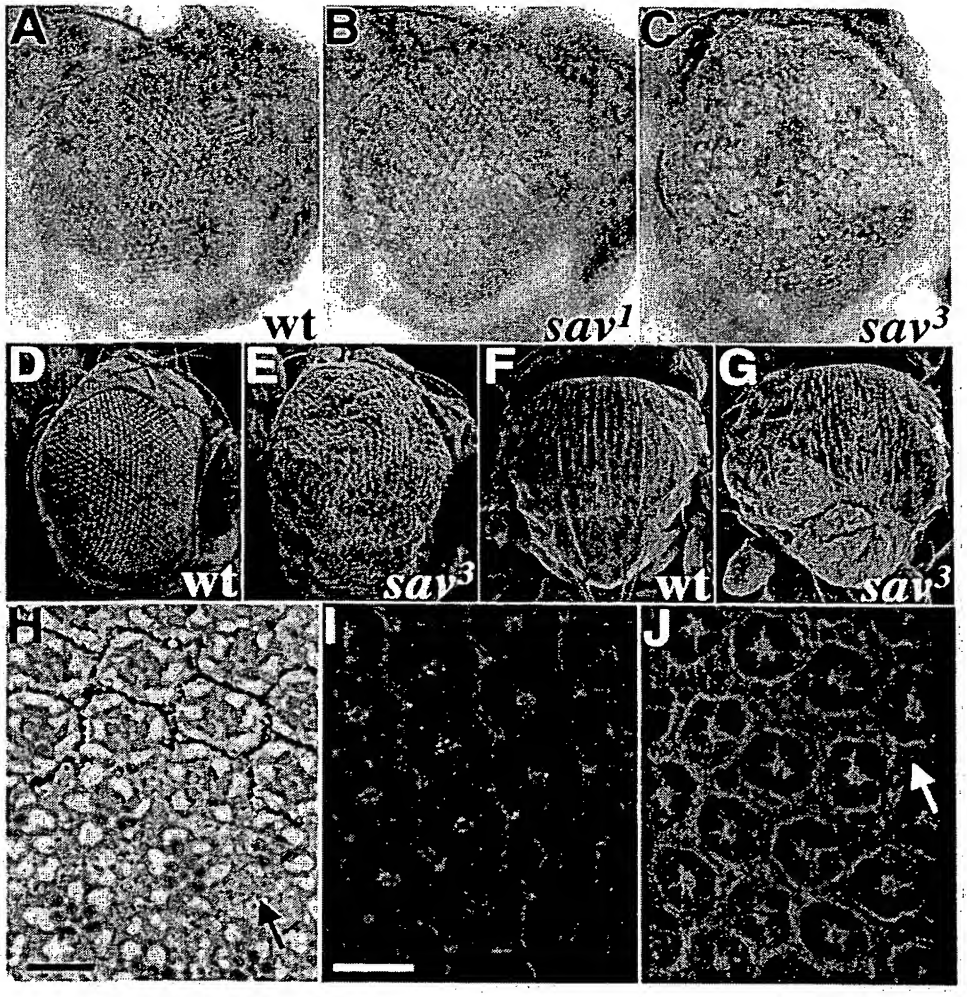

Figure 1. *sav* Mutations Result in Increased Growth Characterized by an Increase in Cell Number

(A–C) Adult eyes containing many homozygous clones of either the parent chromosome with the *FRT82B* P element (A), the sav^1 allele (B), or the sav^3 allele (C). Both *sav* alleles result in an increased representation of mutant (white) tissue over wild-type (red) tissue.

(D–G) Scanning electron micrographs of the eye (D) and notum (F) of wild-type flies and of flies that have sav^3 mutant clones (E and G).

(H) Adult retinal sections showing sav^1 clones. The mutant tissue lacks pigment. Mutant clones have excessive tissue (arrow) between adjacent ommatidia.

(I and J) Phalloidin-stained eye discs from 46 hr pupae (at 25°C) shows a single layer of interommatidial cells in the wild-type disc (I) and many additional interommatidial cell outlines (arrow) in *sav* clones (J). The mutant clone in (J) fails to stain with anti-β-galactosidase (green). Scale bars in (H) and (I) equal 10 μm.

Cell Immediate Early Publication

Published Online July 12, 2002
DOI: 10.1016/S0092867402008243

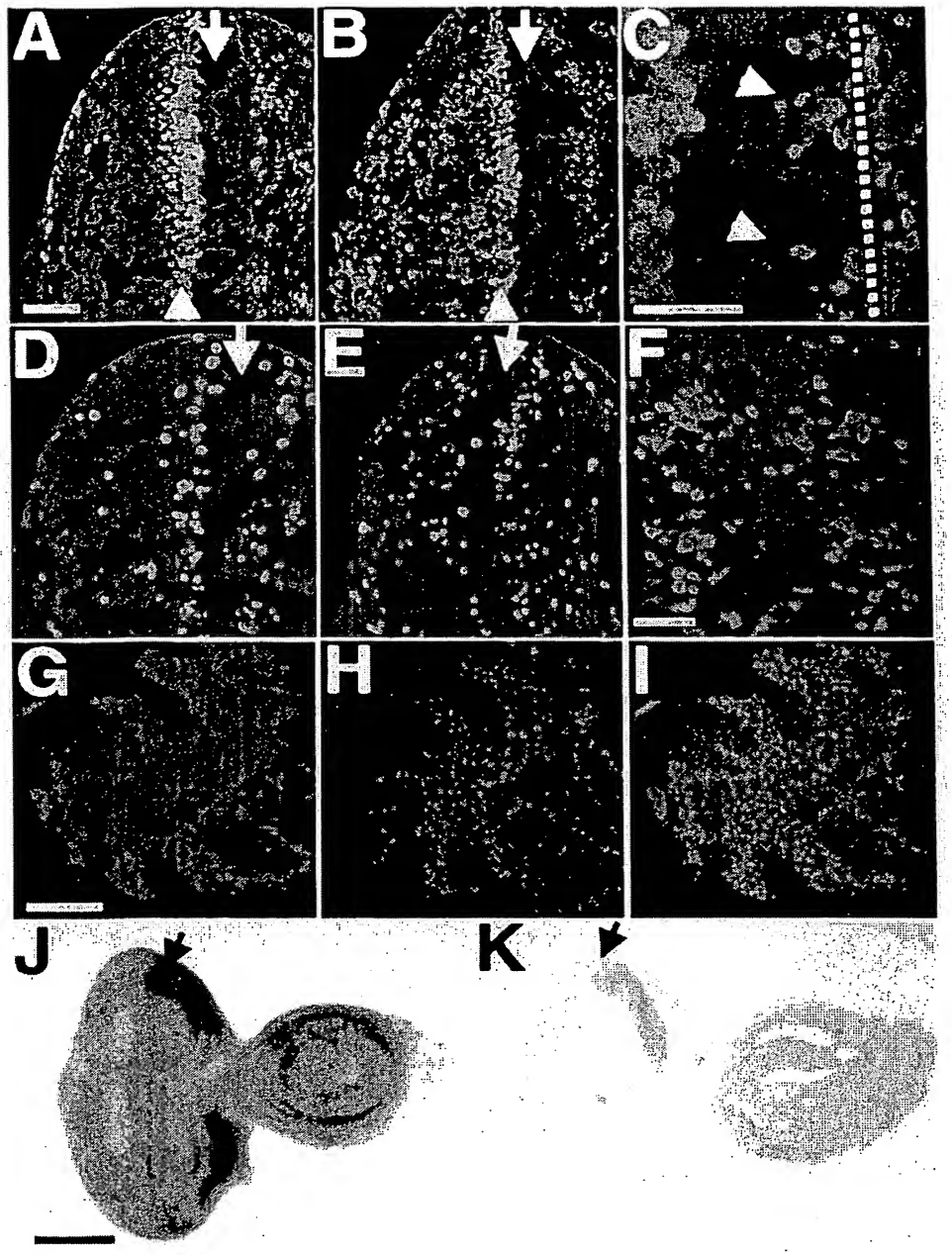

Cell Immediate Early Publication

Published Online July 12, 2002
DOI: 10.1016/S0092867402008243

Figure 2. *sav* Mutations Delay Cell Cycle Exit and Prevent Apoptosis in the Eye Imaginal Disc

(A–E, J, and K) Eye imaginal discs from third instar larvae. Anterior is to the right. In (A)–(E), the mutant tissue fails to stain with anti-β-galactosidase (green).

(A–C) BrdU incorporation (red) in discs containing clones of homozygous tissue of the parent chromosome (A) or the sav^3 allele (B and C). In wild-type discs (A), a single band of BrdU incorporation, the SMW (arrowhead), is evident posterior to the MF (arrow). In discs containing *sav* clones (B), BrdU incorporation occurs posterior to the SMW.

(C) A sav^3 clone that spans the MF at high magnification shows S phases within the furrow (arrowheads). The dotted line indicates the anterior margin of the MF.

(D and E) Mitoses visualized with the anti-phospho H3 antibody in a disc containing clones of the parent chromosome (D) or sav^3 (E). Arrows indicate the MF.

(F) Imaginal disc from a 12 hr pupa showing BrdU incorporation in sav^3 clones when wild-type discs (not shown) do not incorporate BrdU.

(G–I) Imaginal discs from a 38 hr pupa. 38 hr pupal retinas containing mutant sav^3 clones (G) that do not stain with anti-β-galactosidase (green). Cell deaths (H) visualized by TUNEL (red).

(I) Merge of (G) and (H) shows apoptosis mostly confined to wild-type cells.

(J and K) Expression of *sav* RNA in a wild-type disc (J). Control hybridization with a sense-strand probe is shown (K).

Scale bar for (A), (B), (D), and (E) equals 50 μm; for (C) and (F), 25 μm; for (G)–(I), 100 μm; and for (J) and (K), 100 μm.

Cell Immediate Early Publication

Published Online July 12, 2002
DOI: 10.1016/S0092867402008243

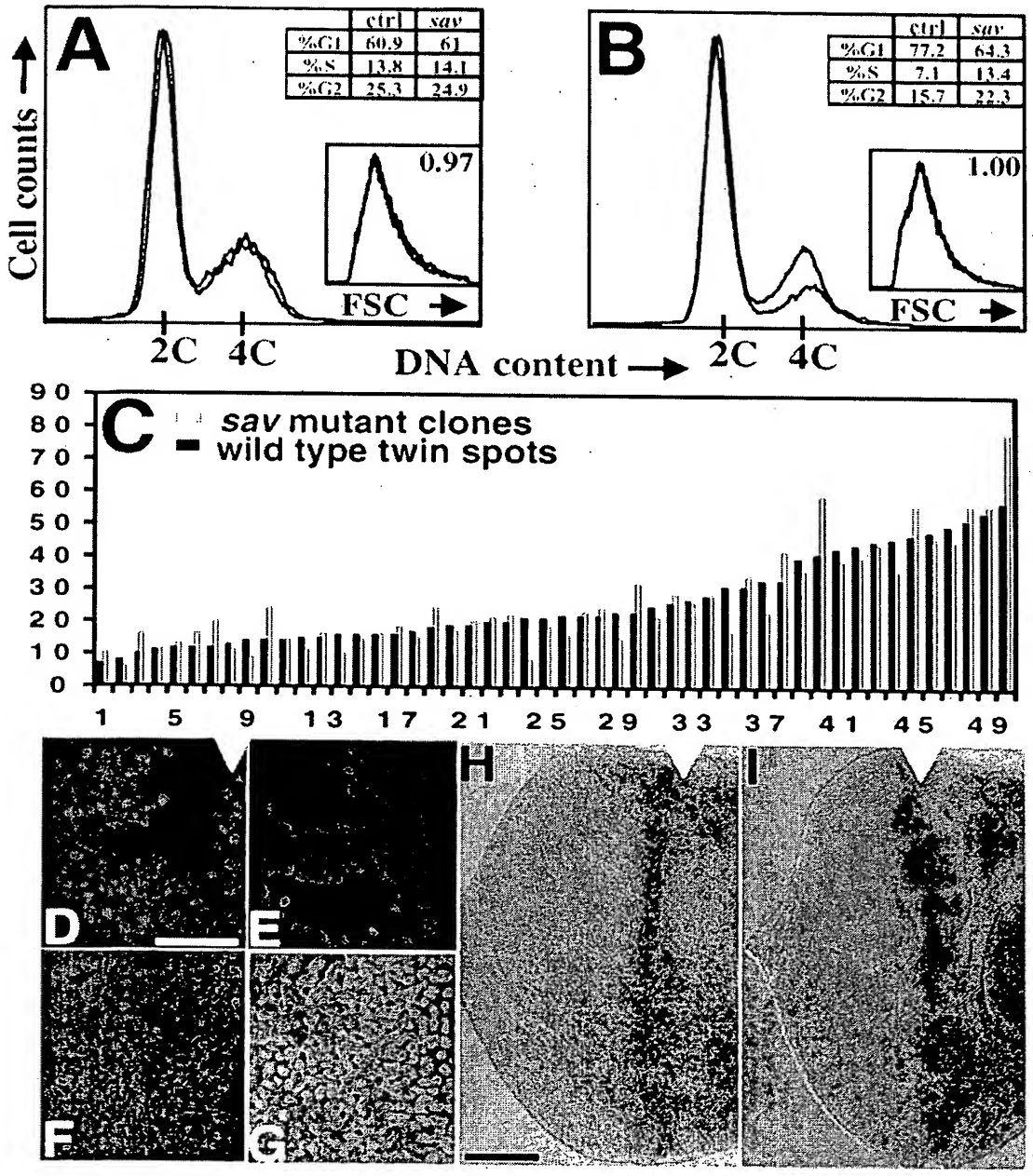

Cell Immediate Early Publication

Published Online July 12, 2002
DOI: 10.1016/S0092867402008243

Figure 3. Cell Cycle Exit Is Delayed in *sav* Mutant Cells

(A and B) DNA content of wild-type (red) and *sav* mutant cells (blue) is similar in early third instar eye antennal discs (96 hr AED) (A). However, in cells from the posterior fragment of eye discs cut at the MF at 124 hr AED (B), an increased proportion of mutant cells is found with a >2C DNA content. Insets show forward scatter (FSC) profiles. The mean FSC of the mutant population compared to wild-type cells is indicated.

(C) Number of cells in individual clone and twin-spot pairs arranged in order of increasing number. Clones were induced in the wing imaginal disc at 48 hr AED and fixed and counted at 120 hr AED. In a student's t test, two-tailed $p = 0.82$, indicating that the number of cells in wild-type and mutant clones is not significantly different.

(D–G) High-magnification images of eye imaginal discs from third instar larvae posterior to the MF focused at the level of the basal nuclei. Elevated levels of Cyclin E (red) in groups of basal nuclei located in *sav* clones (D). *sav* clones (E) fail to stain with anti-β-galactosidase (purple). Nuclei (F) are stained with YOYO1 (green). A merge of these three images is shown in (G). The arrowhead in (D) indicates the stripe of Cyclin E protein expression observed in wild-type discs. Scale bar equals 25 μm.

(H and I) *cyclin E* RNA detected by in situ hybridization in wild-type imaginal discs (H) and discs containing many *ey-FLP*-induced *sav* clones (I). *cyclin E* RNA is expressed at increased levels in mutant discs compared to the narrow stripe of expression observed in wild-type discs. Scale bar equals 50 μm. The arrowhead indicates the MF. Anterior is to the right in (D)–(I).

Cell Immediate Early Publication

Published Online July 12, 2002
DOI: 10.1016/S0092867402008243

Cell

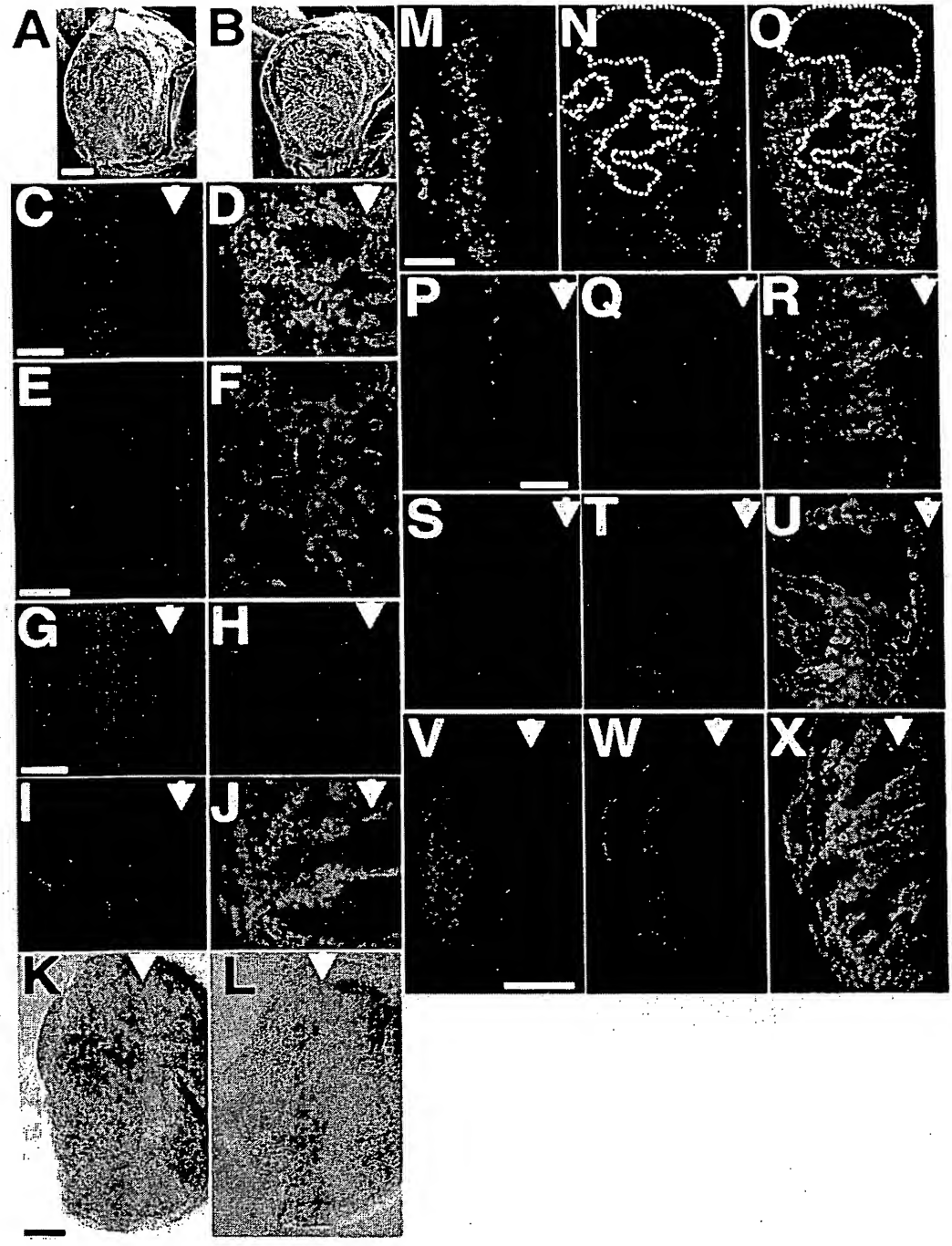

Cell Immediate Early Publication

Published Online July 12, 2002
DOI: 10.1016/S0092867402008243

Figure 4. *sav* Is Required for Normal Developmental Apoptosis and Apoptosis Induced by *GMR-hid*

(A and B) Scanning electron micrographs of adult eyes of flies expressing *GMR-hid* and harboring *eyFLP*-generated clones of wild-type cells (A) or sav^3 mutant cells (B) showing suppression of the *hid*-induced small eye phenotype by *sav*. Scale bar equals 100 μm.

(C–J and M–X) Eye imaginal discs examined for DIAP1 expression (C–J), apoptosis (M–O), or activated Drice (P–X). In all these panels, *sav* clones fail to stain with anti-β-galactosidase (green). Anterior is to the right. The arrow indicates the MF.

(C–J) DIAP1 levels (red) in larval (C and D, G–J) or pupal (E and F) imaginal discs. Elevated DIAP1 levels are found in *sav* mutant clones in the larva (C and D). For the images in (C) and (D), the detector gain in the confocal microscope was reduced, relative to all other images, because of the intense DIAP1 staining in mutant clones. Elevated DIAP1 levels are found in the interommatidial cells in *sav* clones in the pupa at 38 hr APF (E and F). Expression of *GMR-rpr* (H) downregulates DIAP1 levels posterior to the furrow compared to wild-type discs (G). The downregulation of DIAP1 occurs in wild-type cells but not in *sav* clones (I and J). Scale bar for (C), (D), and (G)–(J) equals 50 μm; for (E) and (F), it equals 25 μm.

(K and L) DIAP1 RNA detected by in situ hybridization in a wild-type imaginal disc (K) and in a disc containing *sav* mutant clones (L). In both types of discs, low level of expression was detected posterior to the MF with no evidence of increased expression in discs containing *sav* clones. Scale bar equals 50 μm.

(M–O) Eye imaginal discs from flies expressing *GMR-hid* in wild-type discs (M) or in discs that contain sav^3 clones (N and O). TUNEL staining (red) shows apoptosis is mostly confined to wild-type tissue (green) in mosaic discs (N and O). Some large clones posterior to the MF are outlined (dotted line). Scale bar equals 50 μm.

(P–U) High-magnification images of cells posterior to the MF in discs expressing *GMR-hid* (P–R) or *GMR-rpr* (S–U). In *GMR-hid* discs (P–R), the pattern of Drice activation (red) in wild-type discs (P) or discs containing *sav* clones (Q and R) shows that the band of Drice activation is interrupted in mutant clones. In *GMR-rpr* discs (S–U), the pattern of Drice activation (red) in wild-type discs (S) or discs containing *sav* clones (T and U) shows that the band of Drice activation is interrupted in mutant clones. The arrow indicates the MF. Scale bar equals 25 μm.

(V–X) Larval eye discs stained with anti-active Drice (red). These discs express *GMR-Hid-Ala5* in either wild-type discs (V) or in discs containing *sav* clones (W and X). Drice activation occurs but is reduced in *sav* mutant clones. Scale bar equals 50 μm.

Cell Immediate Early Publication

Published Online July 12, 2002
DOI: 10.1016/S0092867402008243

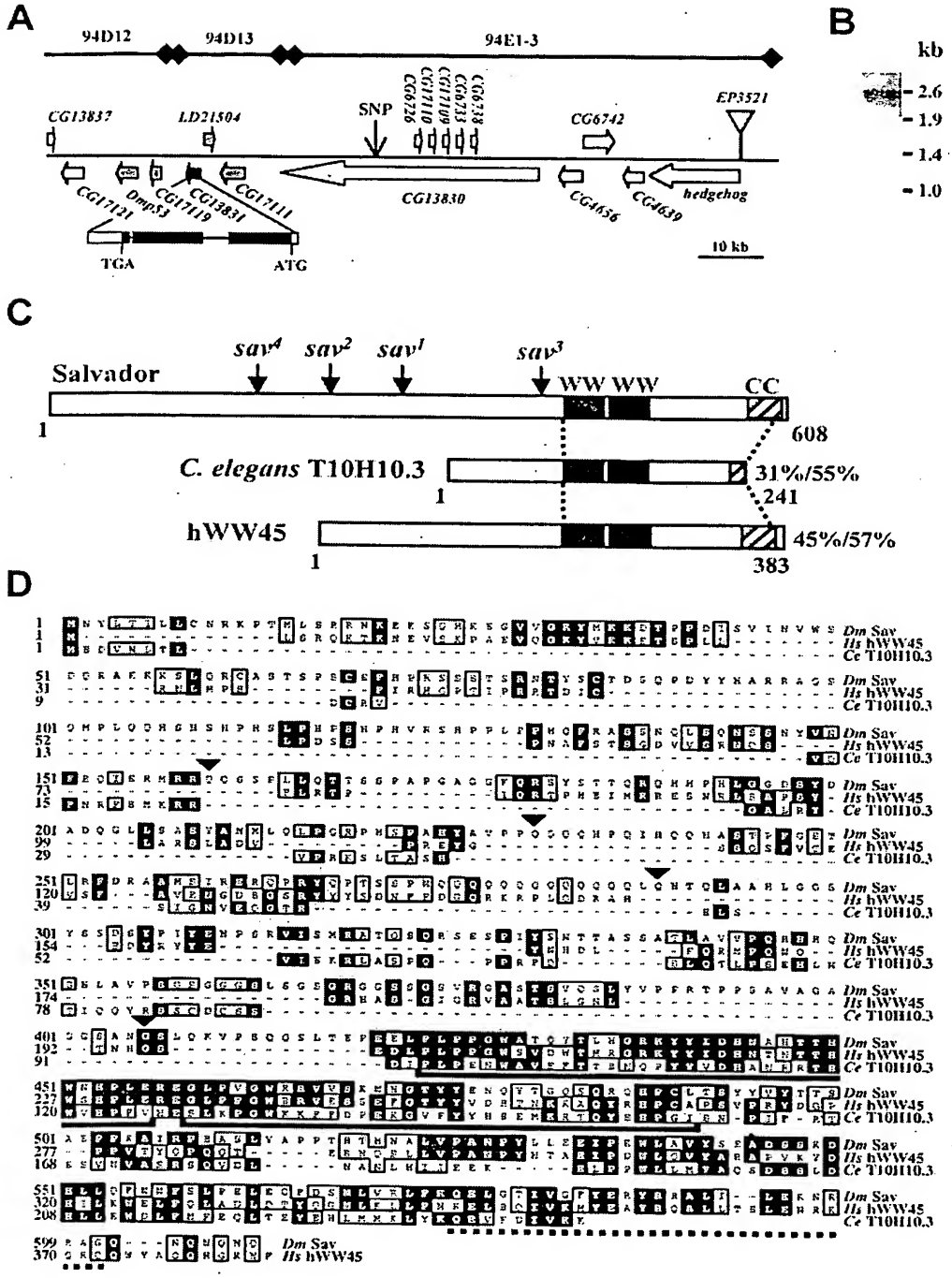

Cell Immediate Early Publication

Published Online July 12, 2002
DOI: 10.1016/S0092867402008243

Figure 5. *sav* Encodes a Protein with Two WW Repeats and a Putative Coiled-Coil Domain

(A) Organization of genes in the vicinity of *sav*. Predicted genes from 94D12 to 94E1-3 are shown (based on Gadfly annotations). *sav* was mapped to the left of EP3521 and to the left of (and close to) a single nucleotide polymorphism (SNP) in CG13830. Open reading frames (ORFs) in the region are represented by arrows. Five ORFs in the vicinity of *sav* were fully sequenced and are shown either as gray arrows or as a black arrow for *sav* (CG13831). Coding regions of *sav* are shown in black, noncoding are in white.

(B) Northern analysis of *sav* mRNA from third instar larval eye discs.

(C) The domain structures of the *Drosophila* Salvador protein, the product of the *C. elegans* open reading frame T10H10.3, and the human protein hWW45. The positions of the *sav* mutations are indicated. WW domains (black) and the putative coiled-coil domain (hatched) are indicated. The similarity of the human and *C. elegans* proteins to *Drosophila* Sav in the region extending from the WW repeats to the C terminus is indicated (identity/similarity).

(D) Amino acid comparisons between the *Drosophila* (*Dm* Sav), human (*Hs* hWW45), and *C. elegans* (*Ce* T10H10.3) proteins. Identical (black box) and similar (open box) residues are indicated. The WW repeats (solid underline), the putative coiled-coil domain (dotted underline), and the locations of mutations in the *Drosophila* Sav protein (arrowheads) are indicated.

Cell Immediate Early Publication

Published Online July 12, 2002
DOI: 10.1016/S0092867402008243

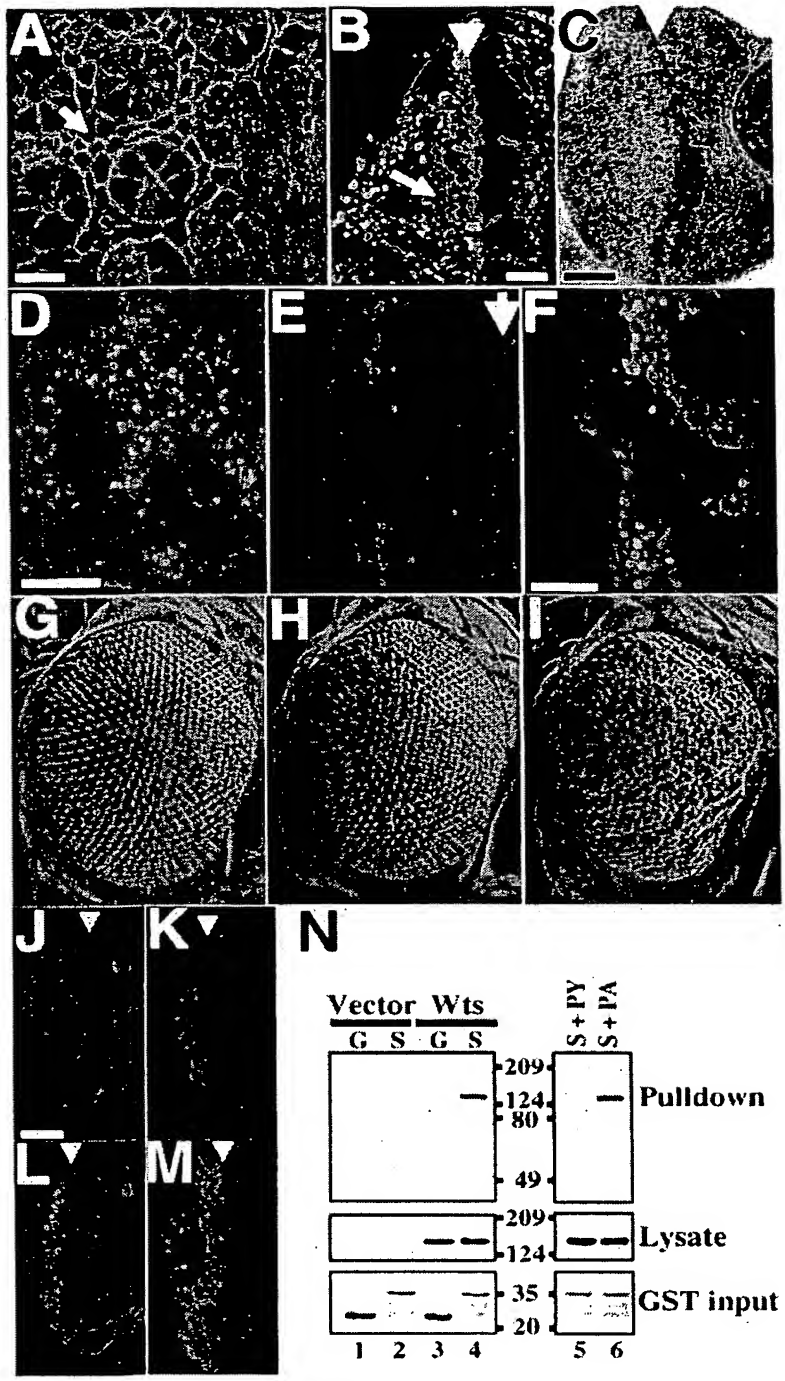

Cell Immediate Early Publication
Published Online July 12, 2002

DOI: 10.1016/S0092867402008243

Figure 6. Genetic Interaction and Physical Association between *sav* and *wts*

(A) Phalloidin-stained (red) 46 hr pupal eye disc shows many additional interommatidial cell outlines (arrow) in clones of wts^{MGH1} tissue. Mutant tissue fails to stain with anti-β-galactosidase (green).

(B) BrdU incorporation (red) in eye imaginal discs from third instar larvae containing clones of cells homozygous for wts^{LATSX1}. The mutant tissue does not stain with anti-β-galactosidase (green). Additional BrdU incorporation (arrow) is visible posterior to the SMW (arrowhead).

(C) Increased expression of *cyclin E* posterior to the MF (arrowhead) is observed in discs containing *wts* clones (compare with Figure 3H). Discs containing *wts* clones are mostly composed of mutant tissue (B).

(D) Disc from 38 hr pupa containing clones of wts^{MGH1}. Mutant clones do not stain with anti-β-galactosidase (red). Cell death visualized by TUNEL (green) is mostly confined to wild-type tissues and hence appears yellow in the merged image.

(E and F) Third instar eye imaginal discs expressing *GMR-hid* in the presence of large *wts* clones. Activated Drice (red) is detected mostly in wild-type tissue that expresses β-galactosidase (green) and is mostly excluded from *wts* mutant clones. The arrow indicates the MF.

Scale bar in (A) equals 5 μm; in (B), 25 μm; and in (C)–(F), 50 μm.

(G–I) Scanning electron micrographs of eyes from male flies of the following genotypes: *GMR-sav/+* (G); *GMR-wts/+* (H); and *GMR-sav/GMR-wts* (I).

(J–M) Overexpression of *sav* and *wts* together in cells posterior to the MF increases cell death. Cell death in third instar eye imaginal discs visualized by TUNEL. Genotypes: +/+ (J); *GMR-sav/+* (K); *GMR-wts/+* (L); and *GMR-sav/GMR-wts* (M). Anterior is to the right in (A)–(M).

(N) Interaction of the Wts protein and the WW domain region of Sav in vitro. Vector- or Wts-transfected cell lysates were incubated with affinity beads loaded with either GST (labeled G) or GST fused to the WW domain region of Sav (labeled S) (lanes 1–4). Wts-transfected cell lysates were also incubated with the WW domain region of Sav in the presence of peptides (1 mM) representing a wild-type (PY) or mutant (PA) PY motif found in the Wts protein (lanes 5 and 6). Wts protein present in cell lysates and bound to the WW domain region of Sav was detected by immunoblotting with anti-Myc. GST fusion protein levels used were assessed by staining with Coomassie blue.

Cell Immediate Early Publication

Published Online July 12, 2002
DOI: 10.1016/S0092867402008243

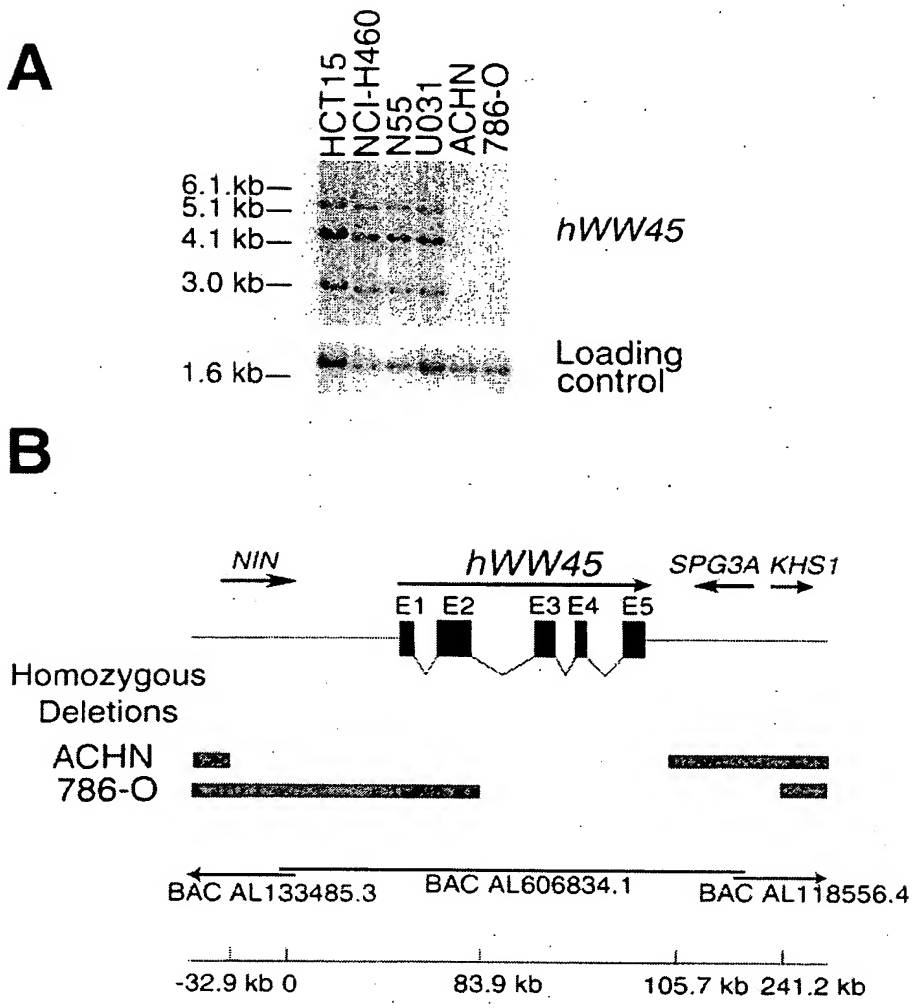

Figure 7. Homozygous Deletion of the *hWW45* Gene in the Human Renal Cancer Cell Lines ACHN and 786-O

(A) Genomic DNA from the renal cancer cell lines, ACHN and 786-O, and control cell lines was digested with EcoRI and hybridized to a cDNA probe corresponding to exons 3–5 of *hWW45* (top). As a loading control, the Southern blot was rehybridized to a cDNA probe for the *WT1* gene (bottom).

(B) Deletion map of the *hWW45* locus in ACHN and 786-O as determined by PCR. The homozygous deletion in ACHN encompasses all five exons of hWW45. The 5′ breakpoint of the deletion in 786-O is between exons 2 and 3, and the deletion extends 3′ of exon 5. On the basis of the GENSCAN exon prediction program, hWW45 is the only gene localized to the region deleted in both cell lines. The positions of other genes (Ninein, Spastic Paraplegia 3A, and Kinase homologous to SPS1/STE20) in the region are indicated in relation to deletion breakpoints and to overlapping BAC clones.

Cell Immediate Early Publication

Published Online July 12, 2002
DOI: 10.1016/S0092867402008243

This Page is Inserted by IFW Indexing and Scanning Operations and is not part of the Official Record

BEST AVAILABLE IMAGES

Defective images within this document are accurate representations of the original documents submitted by the applicant.

Defects in the images include but are not limited to the items checked:

- ☐ BLACK BORDERS
- ☐ IMAGE CUT OFF AT TOP, BOTTOM OR SIDES
- ☑ FADED TEXT OR DRAWING
- ☑ BLURRED OR ILLEGIBLE TEXT OR DRAWING
- ☐ SKEWED/SLANTED IMAGES
- ☑ COLOR OR BLACK AND WHITE PHOTOGRAPHS
- ☐ GRAY SCALE DOCUMENTS
- ☐ LINES OR MARKS ON ORIGINAL DOCUMENT
- ☐ REFERENCE(S) OR EXHIBIT(S) SUBMITTED ARE POOR QUALITY
- ☐ OTHER: _____

IMAGES ARE BEST AVAILABLE COPY.
As rescanning these documents will not correct the image problems checked, please do not report these problems to the IFW Image Problem Mailbox.